Materials Science & Engineering A 687 (2017) 211–220

Contents lists available at ScienceDirect

Materials Science & Engineering A

journal homepage: www.elsevier.com/locate/msea

Dislocation configuration and solute redistribution of low angle kink boundaries in an extruded Mg–Zn–Y–Zr alloy

Z.Z. Peng[a], X.H. Shao[a,*], Q.Q. Jin[a,b], J.F. Liu[a,1], X.L. Ma[a,c,**]

[a] Shenyang National Laboratory for Materials Science, Institute of Metal Research, Chinese Academy of Sciences, 72 Wenhua Road, Shenyang 110016, China
[b] School of Materials Science and Engineering, University of Science and Technology of China, Hefei 230026, China
[c] School of Materials Science and Engineering, Lanzhou University of Technology, Langongping Road 287, Lanzhou 730050, China

ARTICLE INFO

Keywords:
Magnesium alloys
LPSO structure
Kink
Solute redistribution
HAADF-STEM

ABSTRACT

The microstructural and chemical features of deformation-induced interfaces are one of key issues in engineering materials because they determine plastic deformation behavior and thus affect mechanical properties of the materials. Using atomic-resolution high-angle annular dark-field scanning transmission electron microscopy, we characterized deformation-induced low angle kink boundaries (LAKBs) in long period stacking ordered (LPSO) structures in an extruded Mg–2.3Zn–6.6Y–0.56Zr (wt%) alloy. We clarified that the LAKB in LPSO phase consists of an array of <a> dislocations, while the LAKB in Mg interlayers sandwiched between LPSO phases is composed of an array of dissociated <c+a> and/or <a> dislocations. Correspondingly, the former and the latter LAKBs are depleted and segregated with Zn/Y/Zr elements, respectively. I_2 stacking fault (SF) is meanwhile generated in Mg layers, and its energy is evaluated approximately 0.1–1.6 mJ m^{-2}. Deformation-induced LAKBs, the resultant redistribution of solute elements, and precipitated I_2 SFs, are proposed to be responsible for the high strength of extruded Mg alloys containing LPSO structures.

1. Introduction

As increasing requirement of reducing energy consumption in automotive and aerospace industry, developing new types of Mg alloys with high strength, high toughness and high temperature creep strength has become the international consensus. Mg–Zn–RE (RE represents rare earth elements) alloys containing LPSO phases have received considerable attention due to their excellent mechanical properties during the past decade [1–10]. The LPSO phase is a novel precipitate, whose basal plane is parallel to that of Mg matrix and its stacking periodicity is lengthened to x-fold along the c-axis (x represents the stacking number in each periodicity) [11–14]. 18R- and 14H-LPSO are the dominant LPSO phases observed in Mg–Zn–RE ternary system [13,14], which are actually made up of two and three AB′C′A-type FCC building blocks, respectively [15,16]. Among them, B′ and C′ layers are enriched of Zn/RE elements [17,18]. LPSO phases always sandwich Mg layers of several to hundreds of nanometers, and then form an LPSO structure. Various deformation process and heat treatment were carried out to further improve the mechanical properties of Mg alloys containing LPSO phase. Specifically, the extruded Mg alloys containing LPSO exhibit good mechanical properties [4–8]. For instance, high tensile yield strength of 345 MPa and elongation of 6.9% could be attained for extruded Mg–Gd–Zn alloys [4], and 390 MPa and 5% for extruded Mg–Y–Zn alloys [5].

Previous studies indicate that high strength of extruded Mg alloys containing LPSO phase has much to do with deformation bending [3,4] or kinking [5,19] of the LPSO phases, in addition to the fine and high dispersed LPSO structure and Mg grains. More work about deformation microstructure has been concentrating on the dislocation-associated kinks. The lattice of the 18R-LPSO structure can rotate about the $<1\bar{1}00>$, $<0\bar{1}10>$, $<0001>$, and $<1\bar{2}10>$ axes in an $Mg_{89}Zn_4Y_7$ alloy extruded at 450 °C, where kink bands with corresponding Taylor axes are produced through a basal or prismatic <a> slip [20]. Micro-kinking in the LPSO grains in a hot-extruded $Mg_{97}Zn_1Y_2$ alloy is proved to be composed of multiply segmented kink-interfaces [21]. And the kink-interfaces and the junctions of the interfaces are composed of <a> and <c>-component dislocations, respectively. Further, the deformation-induced dislocations and kinks

* Corresponding author.
** Corresponding author at: Shenyang National Laboratory for Materials Science, Institute of Metal Research, Chinese Academy of Sciences, 72 Wenhua Road, Shenyang 110016, China.
E-mail addresses: xhshao@imr.ac.cn (X.H. Shao), xlma@imr.ac.cn (X.L. Ma).
[1] Current address: The Molecular Foundry, Lawrence Berkeley National Laboratory, Berkeley, CA 94720, USA.

http://dx.doi.org/10.1016/j.msea.2017.01.088
Received 25 November 2016; Received in revised form 20 January 2017; Accepted 23 January 2017
Available online 24 January 2017

have been suggested to be accompanied by the redistribution of solute atoms in matrix and LPSO structures. For example, the extended < a > dislocations are indicated to be associated with segregation and depletion of Zn/Y elements at the stacking faults in Mg and in LPSO phase in an extruded $Mg_{97}Zn_1Y_2$ alloy, respectively [22]. Low and high angle kink boundaries in LPSO phases of Mg–Zn–Y alloys are suggested to segregate with Mg and Zn/Y elements, respectively, which are rationalized by the proposed dislocation constructions in the LPSO phase [23–25]. These experiments strongly imply that there's an intimate relationship between the kink boundaries with unique dislocation configurations and chemical redistribution in LPSO structures upon deformation, which may unravel the strengthening nature of LPSO phases in extruded Mg alloy. However, atomic-scale insights of the deformation-induced kink boundary and associated chemical composition of LPSO structures are not clarified so far, leaving a big gap to achieving a desired performance by optimizing process parameters.

By thoroughly characterizing the microstructural and chemical features of deformation-induced interfaces in materials at atomic level, the aim of our study is to contribute to a better understanding of the strengthening mechanism of extruded Mg alloys containing LPSO structure. Here we provided a direct visualization of deformation-induced LAKBs in the LPSO structures and I_2 stacking faults (SFs) precipitated in Mg interlayers during extrusion in a hot-extruded Mg–2.3Zn–6.6Y–0.56Zr (wt%) alloy, using atomic-resolution high-angle annular dark-field scanning transmission electron microscopy (HAADF-STEM). The solute redistribution along LAKBs was distinguished based on the special dislocation configurations of LAKBs. The strengthening effects of deformation microstructure of LPSO structures on Mg alloys were also discussed.

2. Materials and methods

A magnesium alloy with the nominal composition of Mg–2.3Zn–6.6Y–0.56Zr (wt%) was produced by an ordinary resistance furnace under mixed gas (99% CO_2+1% SF_6) atmosphere. The ingot was homogenized at 525 °C for 24 h, and then extruded into a bar with a sectional area 16 mm×30 mm. The extrusion temperature and extrusion ram speed were 450 °C and 1.0 mm s^{-1}. The extrusion ratio was approximately 13. After grinding and polishing, microstructure examination was conducted firstly in optical microscope and scanning electron microscope (SEM; LEO, Oberkochen). Samples used for transmission electron microscopy (TEM) observation were cut into 0.7 mm thick slices using low speed saw cutting machine by water cooling. After grinding and dimpling, thin foil samples were ion milled by a Gatan precision ion polishing system (PIPS 691) with a liquid-nitrogen-cooled stage to avoid preferential thinning effects. A Titan^{3TM} G^2 60-300 aberration-correction TEM, equipped with an HAADF detector, energy-dispersive X-ray spectrometer (EDS) systems, operated at 300 kV, was used for microstructural and compositional investigations. Note that in this work the observation direction of the extrusion samples is parallel to the elongation direction. That is, the observation plane is the normal-transverse plane.

3. Results

3.1. Homogenizing-treated and hot-extrusion microstructure of Mg–Zn–Y–Zr alloy

Fig. 1a provides an optical microscope image of the homogenizing-treated Mg–Zn–Y–Zr alloy, indicating the microstructure consists of equiaxed Mg grains with profuse line contrast (solid arrows) and strip-shaped LPSO structures at the grain boundaries (open arrows). The sizes of matrix grain and intercrystalline LPSO structures were evaluated and listed in Table 1. The LPSO phases could exist as thin plates in the matrix, and may sandwich Mg interlayers or exist individually at the grain boundaries. The average chemical composition of the Mg (including Mg matrix and sandwiched Mg interlayers) and the intercrystalline LPSO phase were determined to be approximately

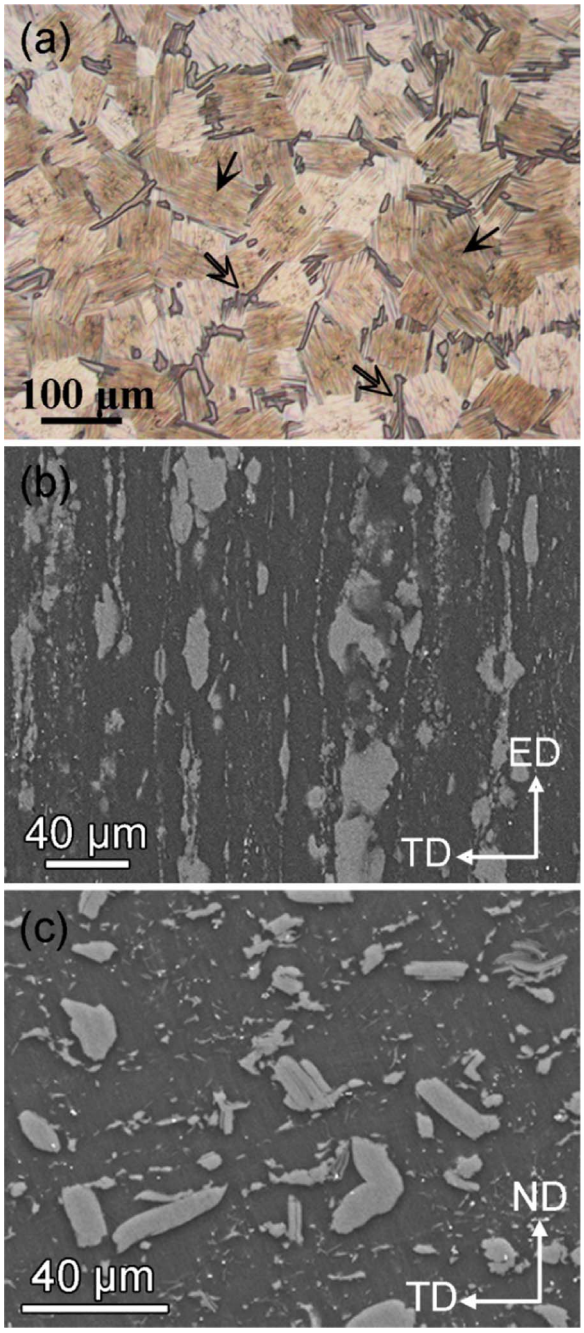

Fig. 1. Homogenizing-treated and hot-extrusion microstructure of Mg–Zn–Y–Zr alloy. (a) Optical microscope image of homogenized sample, where the Mg matrix and intercrystalline LPSO phases are indicated by the solid and open arrows, respectively. SEM images of (b) longitudinal and (c) transverse sections of the hot-extruded sample where the LPSO phases exhibit bright contrast. Here, ED, TD and ND represent the extrusion, transverse and normal direction, respectively.

Table 1
The sizes of matrix grain and intercrystalline LPSO phase in homogenizing-treated Mg–Y–Zn–Zr alloy.

	Size range/μm	Average size/μm
Mg matrix grain	24–85	51 ± 16
LPSO structures	4–37	10 ± 6

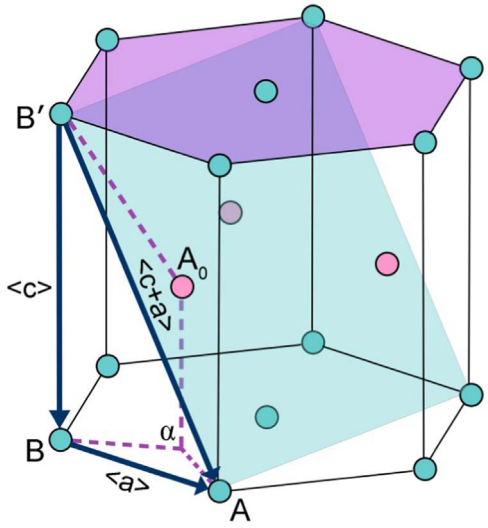

Fig. 2. A schematic diagram of Burgers vectors in HCP lattice, showing < a > , < c > , < c+a > , and some partial dislocations.

Mg–0.04Zn–0.71Y–0.19Zr (at%) and Mg–7.89Zn–5.82Y–1.65Zr (at %), respectively, using TEM-EDS. Fig. 1b and c show the SEM microstructure of longitudinal and transverse section of extrusion specimen, respectively, where the LPSO phase exhibited bright contrast and Mg matrix dark contrast under the back scattered electron imaging condition. One can see that LPSO phase of various widths is aligned along extrusion direction (Fig. 1b), while LPSO phase distributes uniformly and many of them curved (Fig. 1c). Hence, in the following we would analyze the transverse section of the sample at the atomic level, in order to unravel the deformation characters of the LPSO structures during extrusion. Further, the chemical composition of the matrix, the LPSO phase and the Mg interlayers sandwiched within LPSO phase after hot-extrusion were evaluated, which had almost no change with respect to the homogenizing-treated specimen.

3.2. Microstructural and chemical features of LAKBs in Mg–Zn–Y–Zr alloy

Fig. 2 shows a schematic diagram of Burgers vectors in HCP lattice which is convenient for describing various dislocations in Mg. Vectors BA, B′B and B′A represent perfect < a > , perfect < c > and perfect < c +a > dislocations, respectively; vectors αA$_0$, αA (αB), and B′A$_0$ represent partial dislocation with Burgers vector of $\frac{1}{2}\langle 0001\rangle$, $\frac{1}{3}\langle 10\bar{1}0\rangle$, and $\frac{1}{6}\langle 20\bar{2}3\rangle$, respectively. The basal and pyramidal $\{11\bar{2}2\}$ plane are highlighted by purple and blue color.

3.2.1. LAKBs in individual LPSO grains

A typical bright-field (BF) TEM image of the deformed LPSO grain in the extruded Mg–Zn–Y–Zr alloy, recorded along $[11\bar{2}0]_{Mg}$ zone axis, is shown in Fig. 3a. It clearly demonstrates that the LPSO phase was bent during deformation, different from the straight LPSO structures before deformation [26]. Fig. 3b and c are the BF-TEM and corresponding HAADF-STEM images of the bended LPSO phase recorded along $[11\bar{2}0]_{Mg}$ orientation, where lots of LAKBs can be observed, as indicated by the arrows. These LAKBs in the LPSO grain, which are also named “micro-kinking” [21], account for the small bending of the LPSO phase. Although the rotation angle of each LAKB in this LPSO grain is less than 5°, the total angle could reach as high as 19°, since all the LAKBs in Fig. 3b and c made the basal planes rotate in a clockwise from left to right.

Fig. 4a demonstrates the magnified HAADF-STEM image of a 3° LAKB in LPSO phase (location “1” in Fig. 3c), which consists of dominant 14H-LPSO and a few 18R-LPSO interlayers (indicated by arrow heads). Fig. 4b is the atomic-resolution HAADF-STEM image of the rectangular area outlined in Fig. 4a. As can be seen from the surrounding Burgers circuits, the LAKB is composed of an array of orderly arranged < a > dislocations, which are vertically arranged to the basal planes. In detail, two kinds of < a > dislocations account for the LAKB. One is extended < a > dislocations, where heavy elements obviously deplete on the B′ and C′ layers, not indicated by any symbol in Fig. 4b. The other is perfect < a > dislocations, where no depletion of heavy elements can be detected on the B′ and C′ layers, marked by the symbol “T” in Fig. 4b. The difference between extended < a > dislocation and perfect < a > dislocation is that the former change FCC “ABCA” stacking sequence into HCP “ABAB” stacking sequence free of heavy elements, while the latter can only bring an extra half plane without any change of solute atoms. In addition, solute atoms segregate at the ends of the area where solutes deplete, since solute atoms tend to diffuse along the basal planes [27]. The rotation angle of the LAKB closely depends on the spacing of the < a > dislocations aligned along c-axis. It can be thus expected that as the angle increases, the spacing between two adjacent dislocations would decrease and the dislocations may occur at two adjacent FCC blocks.

Interestingly, the dislocation configuration of the LAKB near the outside edge of the bended LPSO grain (location “2” in Fig. 3c) is a little bit different from the situation shown in Fig. 4. As presented in Fig. 5a, there's no apparently dark contrast along LAKB. The atomic-resolution HAADF-STEM image in Fig. 5b demonstrates that no extended < a > dislocation but all perfect < a > dislocations can be detected in this segment, where the extra half planes are indicated by the “T” symbols. Therefore, there's no apparent depletion of heavy elements on the B′ and C′ layers. The reason of no extended dislocations here may be interpreted as follows: The SF energy of the LPSO phase is relatively high, which can be confirmed by the short widths of the SFs in LPSO phase, as shown in Fig. 4. A large stress is thus required to dissociate the perfect < a > dislocation, which is consistent with the twinning phenomenon in pure Al [28]. Since the stress in the perimeter of the bended LPSO can be partly released by the adjacent Mg grain, the residual stress here is not enough to promote the dissociation of the perfect < a > dislocation. Fig. 5c–e show the dislocation cores of the perfect < a > dislocations, where the atoms on extra half-planes are indicated by the red dots. Most dislocation cores lie in the B′and C′ layers, as marked by the red dots in Fig. 5c. Only a few dislocation cores are located at the A layers or other Mg layers, as marked by the red dots in images of Fig. 5d and e, respectively. The ratio of dislocation cores distributed at B′ and C′ layers, A layers and other Mg layers is approximately 10:3:2. The fact that the < a > dislocations preferentially existed on the B′ and C′ layers may be suggested that the dislocations can preferentially move on those planes or the formation energy of < a > dislocation is lower on those planes. Although the reason is not clear now, the crystal structure and the atomic species should play an important role.

In addition, the junctions along basal planes with dark contrast between LAKBs are usually observed in deformed LPSO phase, as indicated by the numerals “I” and “II” in Fig. 6a. These junctions of the LAKBs were proved to be composed of < c > -component dislocations using two-beam imaging method [21]. It is hard to understand the microscopic structure of the junctions only by doing so. Therefore, we investigated the dislocation constructions via atomic-resolution HAADF-STEM. Fig. 6b shows two extra half-planes of atoms represented by the symbol “T” in the location “I” in Fig. 6a. The dislocation contains extra < c+a > -component, in addition to an extended < a > dislocation, as indicated by the large Burgers circuit. The < c+a > dislocation dissociates into two basal oriented partial dislocations and both the dislocation cores are segregated with heavy atoms. Fig. 6c demonstrates that an even more complicated dislocation structure associated with six extra half-planes of atoms in the location “II”, represented by the “T” symbol. Combining with the dislocations that do not induce extra half-planes of atoms, the sum of Burgers vectors of all

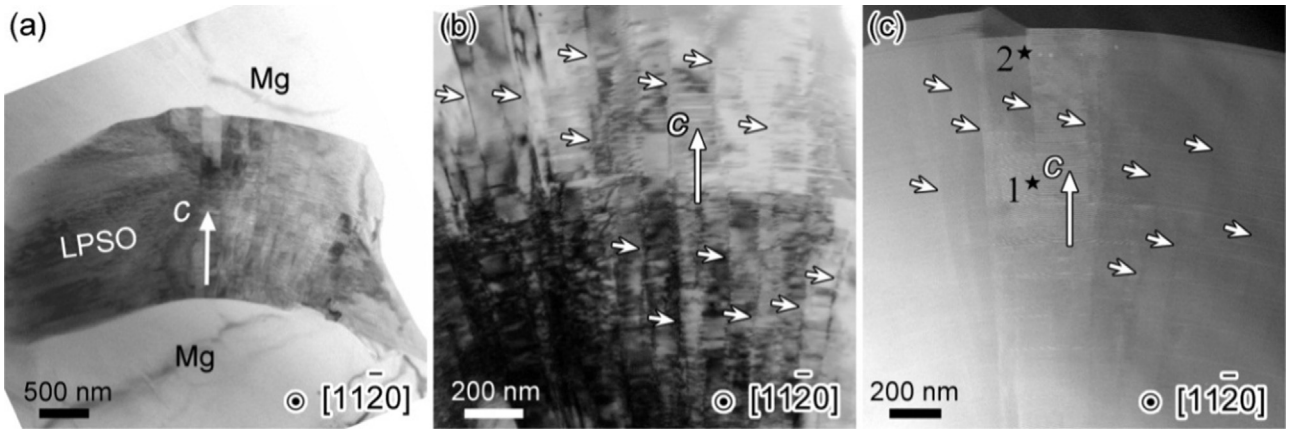

Fig. 3. Morphologies of a bended LPSO grain in the extruded alloy. (a) Bright-field TEM image. (b) Enlarged bright field TEM image and (c) corresponding HAADF-STEM image, where the LAKBs are indicated by the arrows. The electron beam is parallel to $[11\bar{2}0]_{Mg}$.

the dislocations here is $<3c+a+p>$, as indicated by the large Burgers circuit in Fig. 6c. The letter *p* represents the partial $<a>$ dislocation in this article, whose Burger vector is $\frac{1}{3}[10\bar{1}0]$. The formation of the complicated dislocation structure can be understood as follows: the stacking sequences of the observed 14H-LPSO grain is ABAB′C′ACACAC′B′ABA, and thus the unit cell of 14H contains two twin-related FCC building blocks [15]. The left part of the distorted region surrounded by the Burgers circuit contains one more FCC building blocks and two more Mg layers than the right part of the distorted region, leading to a total Burgers vector of $<3c+a+p>$. It should be noted that heavy atoms deplete between the dislocations but enrich in dislocation cores in the location "II", similar to but more complicated than that in location "I". The tilt angles induced by the dislocation structures in "I" and "II" regions are 2.3° and 3°, respectively.

Therefore, LAKBs in individual LPSO grains are associated with extended $<a>$ dislocations depleted with solute atoms and/or perfect $<a>$ dislocations free of solutes depletion. Meanwhile, the junctions

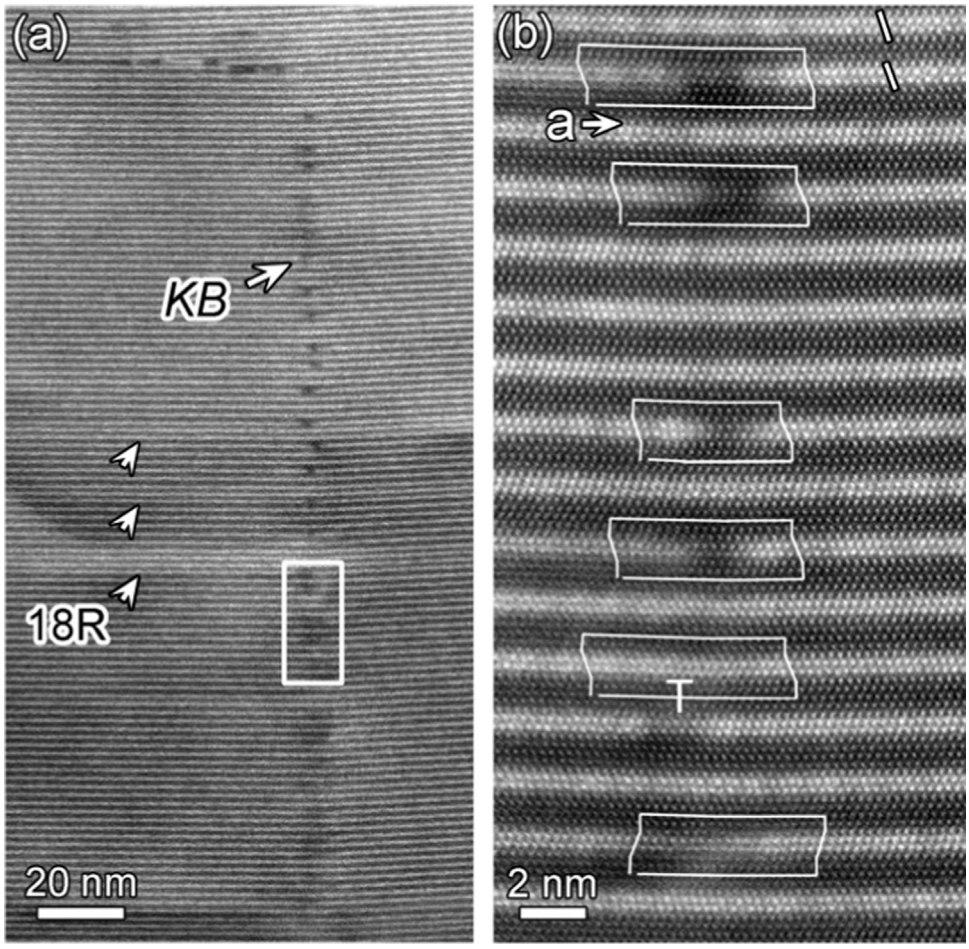

Fig. 4. A LAKB in the bended LPSO grain (location "1" in Fig. 3c). (a) Low-magnification HAADF-STEM image. (b) Atomic-resolution HAADF-STEM image for rectangular region in (a). Burgers circuits are delineated by white lines, which surround five extended $<a>$ dislocations with depletion of solute atoms and one perfect $<a>$ dislocation free of atoms redistribution. The perfect $<a>$ dislocation was indicated by the symbol "T".

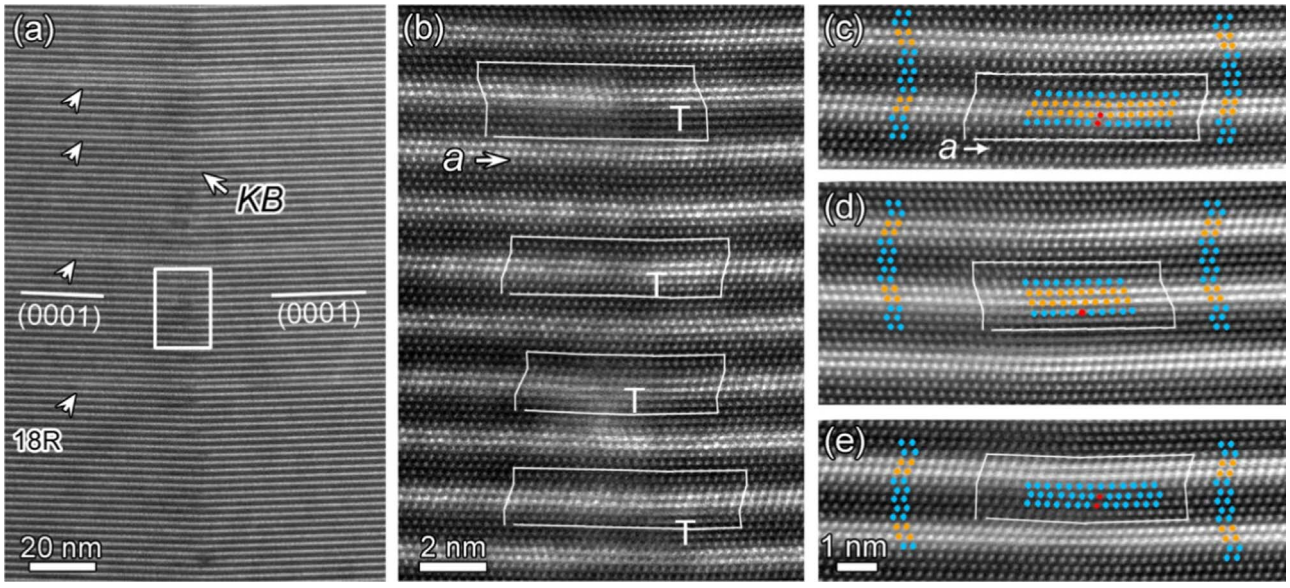

Fig. 5. The LAKB at the outside edge of the bended LPSO grain (location "2" in Fig. 3c). (a) Low-magnification HAADF-STEM image. (b) Atomic resolution HAADF-STEM image of the marked area in (a), showing this LAKB is composed of perfect < a > dislocations, marked by the "T" symbols. Dislocation cores distributed at B′ and C′ layers (c), A layers (d) and other Mg layers (e), where the extra half-plane of atoms are indicated by the red dots. Orange and blue dots represent atoms on B′ and C′ layers and other layers, respectively. (For interpretation of the references to color in this figure legend, the reader is referred to the web version of this article).

between segments of LAKBs contain < c+a > complicated dislocations, and dislocation cores are enriched with solute atoms.

3.2.2. LAKBs in LPSO/Mg intergrowth grains

Fig. 7a is a typical morphology of the LPSO/Mg intergrowth grain after extrusion. Under Z-contrast imaging condition, the LPSO phase and Mg exhibit bright and dark contrast, respectively. Obviously, the $(0001)_{Mg}$ basal planes of the LPSO/Mg grain uniformly bent with a small angle around the $[11\bar{2}0]_{Mg}$ direction. Fig. 7b provides the magnified image of the framed area by a square in Fig. 7a. One can see many bright lines of various lengths in the Mg interlayers: some of them are distributed randomly, and some of them are aligned vertically in specific regions, marked by the white arrows. According to our further atomic-scale investigation, the bright lines are proved to be extended < a > dislocations segregated with Zn/Y/Zr heavy elements, I_2 SFs, which is consistent with the descriptions of Hiraga et al. [22]. On the other hand, only a few of LAKBs can be observed in the LPSO phase, as indicated by the black arrows. These KBs are proved to be composed of arrays of orderly distributed < a > dislocations, which are vertical to the basal planes. To be sure, this dislocation structure of the LAKBs is same as that in individual LPSO grains (Figs. 4 and 5).

In some other regions, the bended LPSO/Mg intergrowth grains with locally larger curvature can be observed, as shown in Fig. 8a. As provided by the enlargement of one of these highly curved areas in Fig. 8b, LAKBs occur not only in the LPSO phases but also in the Mg interlayers, indicated by the arrow heads. To thoroughly understand the dislocation structure of this kind of LAKB, a local area "1" containing an LAKB is enlarged and shown in Fig. 9a. It demonstrates that the interface is not straight and enriched with heavy elements. Fig. 9b and c are the atomic-resolution images of regions "I" and "II" in Fig. 9a, respectively. In Fig. 9b, the LAKB is composed of three pairs of orderly arranged dissociated < c+a > dislocations, indicated by symbol "T", and numbers of orderly arranged extended < a > dislocations. Each pair of dissociated < c+a > dislocations is artificially surrounded

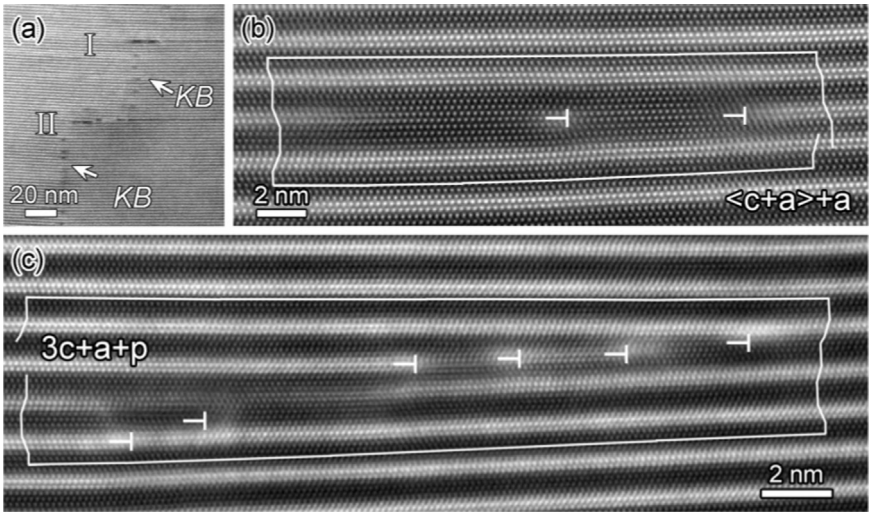

Fig. 6. Microstructure of the junctions of the LAKBs. (a) Low-magnification image showing elongated dark contrasts along basal planes, denoted by "I" and "II". Atomic resolution images for region "I" (b) and "II" (c) in (a), respectively, indicating the junctions are composed of complicated dislocation structures. Burgers circuits are delineated by the white lines, and the extra half-planes of atoms are denoted by the symbols "T".

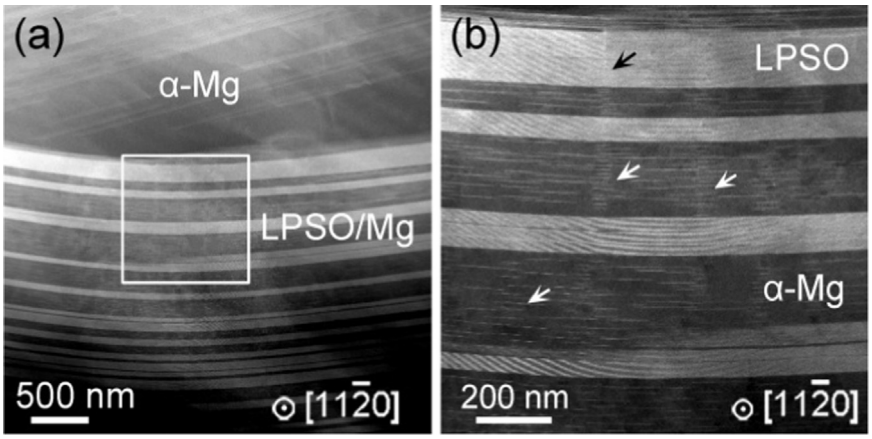

Fig. 7. Typical morphologies of the deformed LPSO/Mg intergrowth grain. (a) Low-magnification image. (b) Enlargement of the framed region in (a), demonstrating extended < a > dislocations segregated with Zn/Y/Zr atoms in Mg layers (white arrows) and a few of LAKBs in LPSO phase (black arrow).

by a white rectangle, one of which is magnified and inserted in Fig. 9b. The < c+a > dislocation would dissociate into two new basal oriented partial dislocations, and be separated by a basal I_1 SF, which is analogous to the situation in pure Mg [29,30]. In the vicinity of the dislocation cores, Cottrell atmosphere is formed, as proved by the apparent concentration of heavy elements. Likewise, "Suzuki effect" can also be observed since the entire orderly arranged extended < a > dislocations are segregated with heavy elements, as indicated by the arrow heads in Fig. 9b and c. It should be mentioned that an arrow head represents an extended < a > dislocation, otherwise, no dislocation exists.

In LPSO/Mg intergrowth grains, the LAKB in LPSO phase is originated from orderly < a > dislocations, while that in Mg interlayers is formed by < c+a > and < a > dislocations. Fig. 10 provides EDS mapping of LAKBs in intergrowth Mg and LPSO phase. The elements distribution on the LAKBs in Mg interlayers and LPSO phases are approximately complementary. Y/Zn/Zr elements are enriched along the LAKB in Mg interlayer, while they are deficient along the LAKB in LPSO phase. Note that the redistribution of Zn atoms is not so obvious as Y and Zr.

3.2.3. LAKBs in wedge-shaped Mg phases of LPSO grains

Fig. 11a demonstrates an HAADF image of a deformed 18R-LPSO grain of 5 μm thickness containing two large wedge-shaped Mg areas (showing dark contrast), as indicated by the Arabic numbers "1" and "2". The angles of the "1" and "2" wedge-shaped Mg areas are 5.6° and 1.8°, respectively. LAKBs with line-like bright contrast are observed in the middle of the two wedge-shaped areas. Fig. 11b provides an atomic-resolution HAADF-STEM image of the head of LAKB in wedge area "1", indicating a < c+a > dislocation dissociates into two new basal oriented partial dislocations, which is separated by a basal I_1 SF. This's framed by the lower rectangular and illustrated by its magnification (the lower inserted image). There's also a dissociated < c+a > dislocation in the nearby LPSO phase, similar to the head of the LAKB, marked by the upper rectangular and described by its magnification (the upper inserted image). Fig. 11c shows the lower part of the LAKB in wedge area "1", where two pairs of the dissociated < c+a > dislocations are artificially surrounded by rectangles. Hence it is fair to say that the LAKB is composed of an array of orderly arranged < c +a > dislocations, and each of them dissociates into two new basal oriented partial dislocations with an I_1 SF. Moreover, I_2 SF exists between each pairs of dissociated < c+a > dislocations. It should be noted that the nature of LAKB in the wedge area "2" (1.8°) is the same as that in wedge area "1" (5.6°). The tilt degree of these wedged areas is consisted with the evaluated spacing of dislocations. These LAKBs show bright contrast mainly because that both the dislocation cores and I_2 SFs are segregated with heavy elements. The chemical composition of the LAKB in wedge area is provided in Fig. 11d, illustrating that the dissociated < c+a > dislocation arrays are enriched with Y/Zn/Zr atoms.

4. Discussion

4.1. Dissociation of < c+a > dislocations in LAKBs

Dissociation of < c+a > dislocations are frequently observed in the

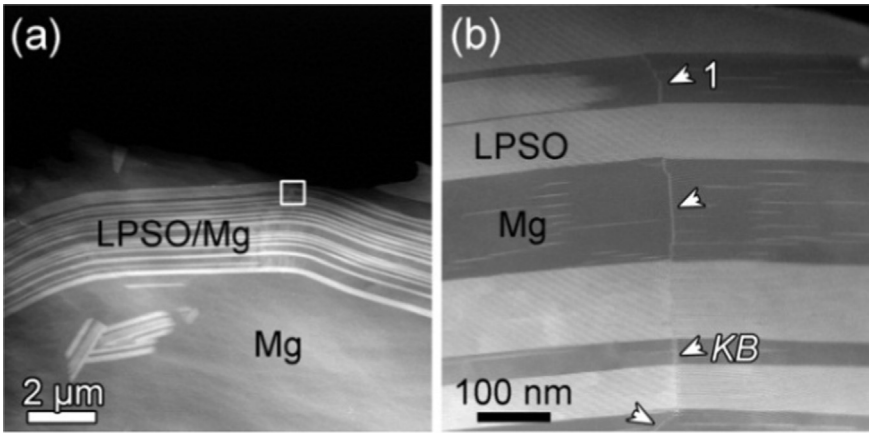

Fig. 8. A deformed LPSO/Mg grain with locally larger curvatures. (a) Low-magnification image; (b) Enlarged image of the marked region by a square in (a), indicating the curvature should be induced by the LAKBs shown by the arrow heads.

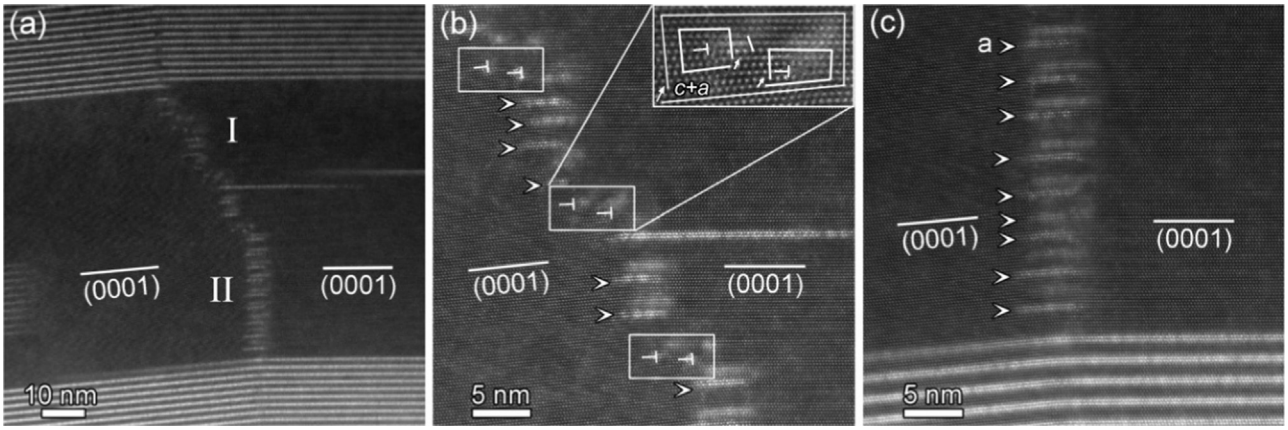

Fig. 9. The LAKB in the LPSO/Mg intergrowth grain. (a) Enlarged image of location "1" in Fig. 8b demonstrates the LAKB consists of complicated dislocation structures enriched with heavy elements. (b) and (c) Atomic resolution HAADF-STEM image of the areas marked by "I" and "II" in (a), respectively, indicating the interface is composed of orderly arranged dissociated < c+a > and < a > dislocations. Three white rectangles outline three dissociated < c+a > dislocations and one is enlarged as inserted, while arrow heads mark < a > dislocations.

LAKBs of the hot-extrusion Mg–Zn–Y–Zr alloys, as evidenced in Figs. 6, 9 and 11. In HCP metals, strain along the c-axis can be accommodated only by twinning and < c+a > slipping [31]. In the present deformed alloy, < c+a > dislocations but no deformation twinning are observed. This can be interpreted from the following aspects. First, due to an increase in the deformation temperature, < c +a > slipping becomes easier than deformation twinning. Máthis et al. [32] proved that above 200 °C, the activation of dislocation motion in the pyramidal system is energetically more favorable than twinning. Second, SFs/LPSO phases in the Mg–Zn–Y alloy can block the propagation of the deformation twinning [33,34]. Meanwhile, the solid solution of Y atoms in the Mg phase, the elastic modulus mismatch between the hard thin LPSO plates and soft Mg phases promote the activation of < c+a > dislocations [34]. Further, it has been documented that < c+a > dislocations have great help to enhance the ductility of the HCP material [35,36] and to improve the formability of wrought magnesium [35,37]. Hence, the orderly arranged < c+a > dislocations in the LAKBs here efficiently coordinated plastic deformation of LPSO structures via making the basal planes tilt around $\langle 11\bar{2}0\rangle_{Mg}$ axis.

Moreover, < c+a > dislocations in the present alloy can further dissociate into two $\frac{1}{6}\langle 2\bar{2}03\rangle$ partial dislocations with an intervening I_1 SF on the basal plane. The dissociation of < c+a > dislocation has been suggested long time ago and further be proved by means of TEM observations [38–40]. Recently, the dissociated < c+a > dislocation was characterized at an atomic scale in STEM [29] and studied using long-time molecular dynamics simulations [30]. < c+a > dislocation was proved to be metastable on easy-glide pyramidal II planes, and it would undergo a thermally activated, stress-dependent transition to one of three lower-energy, basal-dissociated immobile dislocation structures [30]. The dissociated dislocation structure in the present hot-extruded alloy belongs to the first situation that the sample is applied zero or low stresses, resulting in a scenario that a new < c+a > core dissociated on the basal plane and is separated by a basal I_1 SF. This final structure is sessile, inducing dislocation walls or LAKBs when the dislocations are orderly arranged, as shown in Figs. 9 and 11. These boundaries can be pinned firmly there and serve as strong obstacles to the motion of other dislocations.

4.2. Solute redistribution to LAKBs during hot-extrusion

As demonstrated above, the chemical distribution on the newly-formed LAKBs in this work can be divided into two types based on phase difference: The Zn/Y/Zr atoms segregate along the LAKBs in Mg interlayers, while Zn/Y/Zr atoms deplete along the LAKBs in LPSO phases, no matter whether the LAKBs are composed of < a > or dissociated < c+a > dislocations. The redistribution of solute atoms

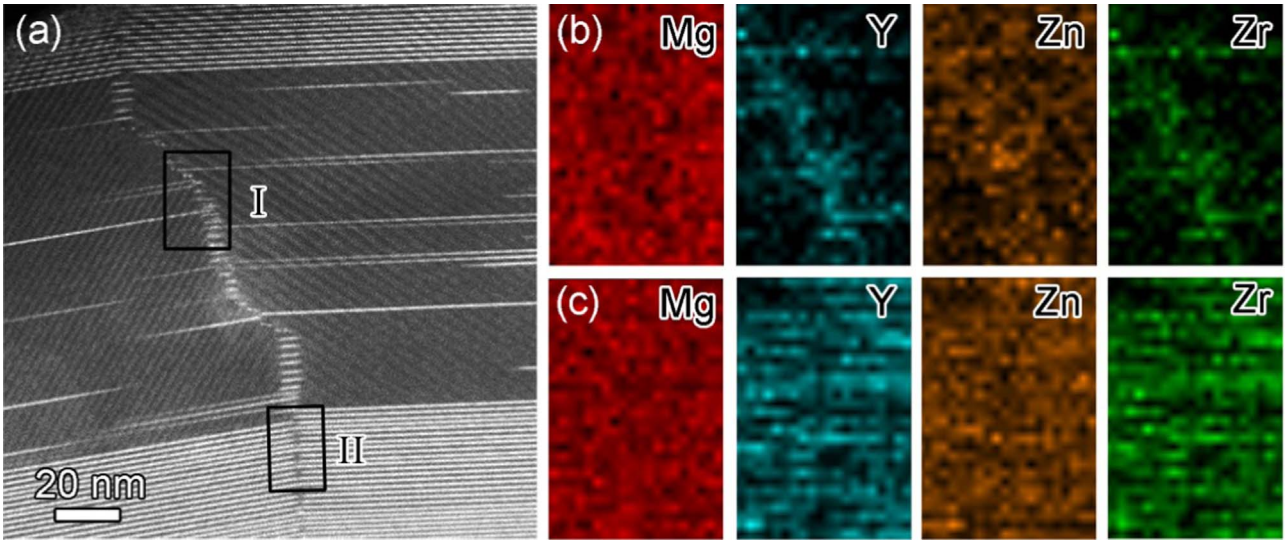

Fig. 10. HAADF-STEM image and EDS mapping of the LAKBs in LPSO/Mg grain. (a) HAADF-STEM image. EDS mapping of LAKB in α-Mg (b) and in LPSO phase (c), proving that the LAKB is enriched with Y/Zn/Zr in the former, but is depleted with Y/Zn /Zr in the latter.

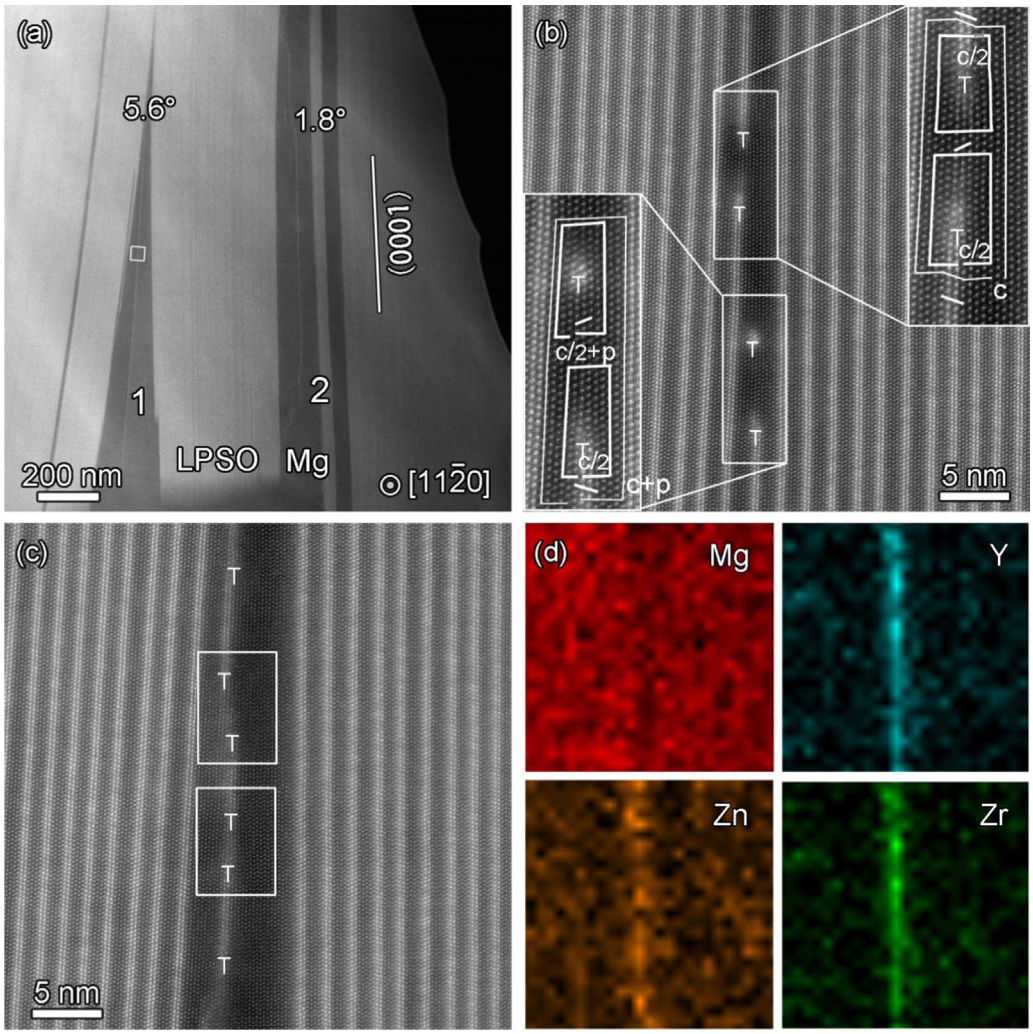

Fig. 11. LAKB in wedge-shaped Mg area and its EDS mapping. (a) An HAADF image of an 18R-LPSO grain containing two wedge-shaped Mg areas indicated by the Arabic numbers "1" and "2". (b) and (c) Atomic resolution HAADF-STEM image for the head and the lower part of the LAKB in wedge area "1", respectively, demonstrating the LAKB was composed of orderly arranged dissociated < c+a > dislocations. Dislocations with the Burgers vector of $\frac{1}{2}$[0001] are marked by the symbols "T". (d) EDS mapping of the LAKB in wedge-shaped Mg phase, framed by a square in (a), showing the LAKB is enriched with Y/Zn/Zr.

induced by plastic deformation may significantly influence mechanical properties of materials [41,42]. The migration of the LAKBs in the Mg interlayers should be greatly inhibited due to the segregated Zn/Y/Zr solute atoms, which is similar to Zn/Y or Mg atoms segregated at kink boundaries in LPSO phase, depending on whether the kinking angle is high or low [23,24]. In what follows we will discuss the nature of solute elements redistribution, which can be explained using traditional Cottrell atmosphere theory [43,44] and Suzuki segregation theory [45]. Solute atoms can be attracted by dislocations to form Cottrell atmospheres, as a result of elastic interaction between dislocations and solute atoms. Similar to Zn/Y Cottrell atmospheres along dislocations at kink boundaries and individual dislocations in bulk LPSO phase [46], we find that Zn/Y/Zr Cottrell atmospheres at $\frac{1}{6}\langle 2\bar{2}03\rangle$ dislocation cores in Mg interlayers in our case. The Cottrell atmospheres can increase the energy barrier for dislocation motion in Mg interlayers during deformation, playing an important role in strengthening the Mg–Zn–Y–Zr material. In analogous to Zn/Y Suzuki segregation in an Mg–Zn–Y alloy [47], we believe that segregation of Zn and Zr is attributed to the chemical interaction between Zn/Zr and the I_2 SFs along the LAKBs, while Y segregation is the result of size effects. The I_2 SF energy was calculated to be about 0.1–1.6 mJ m^{-2} for Mg phase in this Mg–Zn–Y–Zr alloy based on Fig. 7 and the equation in [48], significantly lower than that of pure Mg (30–80 mJ m^{-2} [48]) and the Mg alloy only containing Zn/Y elements (4.0–10.3 mJ m^{-2} [47]). It strongly indicates that the addition of Zr atoms can further lower the SF energy.

The atomic configuration and chemical compositions along LAKBs here are radically different from the kink boundaries in Mg–Zn–Y alloys [25] owing much to the different deformation process, hot extrusion and compression at room temperature. That is, we here assume that motion of dislocations associated with diffusion of solute atoms should be responsible for the big difference. After compression at room temperature, only Zn atoms segregated randomly, form nanoclusters, or distributed periodically along symmetrical KBs in Mg–Zn–Y alloys, where the diffusion of solute atoms induced by the temperature can be ruled out. While during hot-extrusion at 450 °C, all Zn/Y/Zr atoms can co-segregate to I_2 SFs along LAKBs in Mg–Zn–Y–Zr alloy, where diffusion of Zn/Y/Zr atoms originated from high temperature is necessary to be considered. The diffusion coefficients of Zn and Y atoms in lattice can be estimated to be faster by several orders of magnitude at 450 °C than those at room temperature [49,50]. As for Zr, it has the same atomic size as Mg. Diffusion of Zr could be considered as the self-diffusion coefficient of Mg. Combining the diffusion along dislocation motions, all of these solute atoms detected along LAKBs in Mg–Zn–Y–Zr alloys after high temperature deformation is understandable easily.

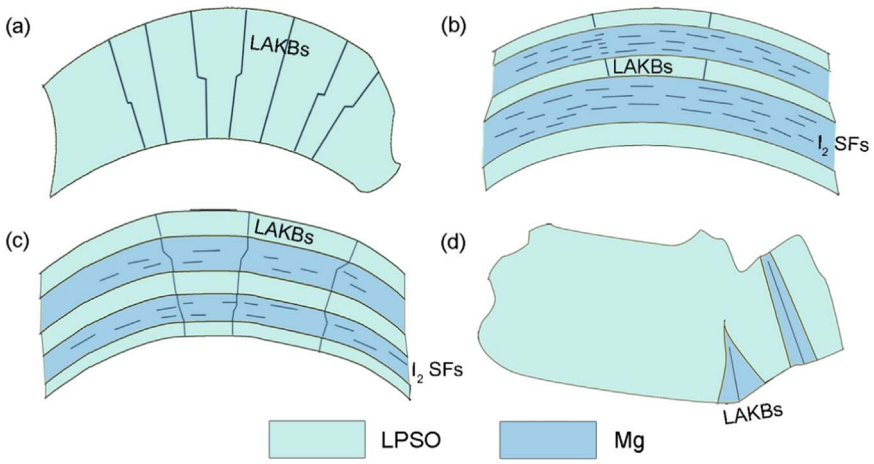

Fig. 12. Schematics of the deformed LPSO structures. (a) LAKBs in an individual LPSO grain; (b) I_2 intrinsic stacking faults precipitated in Mg interlayers of a LPSO/ Mg intergrowth grain; (c) LAKBs run through Mg and LPSO phases of a LPSO/Mg intergrowth grain; (d) LAKBs in wedge-shaped Mg areas of a LPSO grain.

4.3. Impact of LAKBs on mechanical properties of Mg alloys

The LPSO phases associated with lots of LAKBs, rather than high angle kink [10,51,52], are observed in this hot extrusion Mg–Zn–Y–Zr alloy. The microstructural and chemical features of LAKBs should significantly affect mechanical properties of Mg alloy, and here we will propose the possible strengthening mechanism of LAKBs on Mg–Zn–Y–Zr alloy. First, Multiple LAKBs formed in individual LPSO grains, in intergrowth LPSO/Mg structures, and in wedge-shaped Mg areas of LPSO grains, as illustrated in Fig. 12, may not only coordinate the grain deformation but also refine the grain size. Hence, they are beneficial to the improvement of the mechanical properties of hot extrusion Mg alloys [4,5]. Second, deformation-induced redistribution of solute atoms could contribute to the strength of Mg alloys due to the pinning effect of segregated solute atoms on the movement of LAKBs. Segregation of solute atoms on the coherent twin boundaries (CTBs) in Mg alloys was proved to pin the CTBs during annealing [53], and that on the grain boundaries also reduce the grain growth in Mg alloy [54]. Thus the redistribution of solute atoms along LAKBs here is proposed to play a key role in stabilizing and strengthening the LAKBs. Last but not the least, the much lower SF energy induced large amounts of SFs in the Mg phases, and the segregation of Zn/Y/Zr solutes on I_2 SFs, make them more stable and more difficult to slide. Thus they would become obstacles and restrictions of motion of other dislocations.

Combined with the microstructure features of various kinds of kink boundaries in LPSO structures [10,23–25], the atomic experimental results here clarify that the formation parameters, e.g. strain rate and temperature, significantly affect the intrinsic characters of kink boundaries in Mg alloys. The formation process hence has to be considered if we are to properly tailor high or low angle KBs of LPSO structures to achieve desired mechanical properties of Mg alloys.

5. Conclusions

The microstructural and chemical features of unique LAKBs in an Mg–2.3Zn–6.6Y–0.56Zr (wt%) alloy after 525 °C homogenizing and 450 °C hot-extrusion have been investigated using HAADF-STEM at the atomic level. The following conclusions can be drawn:

1. The distinguished LAKBs with various dislocation constructions are generated in the LPSO structures depending on the special location: individual LPSO grains, LPSO/Mg intergrowth grains and LPSO grains containing Mg wedge-shaped areas. First, the LAKBs in the individual LPSO grains and in the LPSO phases of LPSO/Mg intergrowth grains consist of arrays of $<a>$ dislocations, which are arranged vertically to the basal planes. Second, the LAKBs formed in the Mg interlayers of the LPSO/Mg intergrowth grains are composed of arrays of dissociated $<c+a>$ dislocations and/or $<a>$ dislocations, nearly vertical to the basal planes. Third, the LAKBs in the wedge-shaped Mg interlayers of the LPSO phases are associated with arrays of dissociated $<c+a>$ dislocations, which align on the basal planes.
2. The redistribution of solute atoms accompanies the generation of LAKBs during hot extrusion. The chemical features of LAKBs in LPSO structures are intimately related to the special location of LAKBs: The Zn/Y/Zr atoms segregate at the LAKBs in Mg interlayers, while Zn/Y/Zr atoms deplete at the LAKBs in LPSO phases, no matter whether the LAKBs are composed of $<a>$ or dissociated $<c+a>$ dislocations. Meanwhile, I_2 SFs with Zn/Y/Zr elements generate in Mg interlayers of LPSO/Mg intergrowth grain, and the energy of I_2 SF is estimated to be in the range of 0.1–1.6 mJ m^{-2}.
3. The profuse LAKBs in LPSO structures, and resultant segregation of solute atoms, and the I_2 SFs segregated with Zn/Y/Zr atoms in Mg interlayers, are proposed to play a critical role in improving the strength of extruded Mg alloys containing LPSO structures.

Acknowledgements

This work is supported by the National Natural Science Foundation of China (grants 51301177), the National Basic Research Program of China (grants 2014CB921002), the Innovation Fund of IMR (SCJJ-2013-PY-08 & 2015-PY08), and the Fund of SYNL (2015FP18). The authors at SYNL are grateful to B. Wu and L.X. Yang of this laboratory for their technical support on the Titan platform of the aberration-corrected scanning transmission electron microscope.

References

[1] K. Yoshihito, H. Kentaro, I. Akihisa, M. Tsuyoshi, Rapidly solidified powder metallurgy $Mg_{97}Zn_1Y_2$ alloys with excellent tensile yield strength above 600 Mpa, Mater. Trans. 42 (2001) 1172–1176.
[2] Y. Kawamura, M. Yamasaki, Formation and mechanical properties of $Mg_{97}Zn_1RE_2$ alloys with long-period stacking ordered structure, Mater. Trans. 48 (2007) 2986–2992.
[3] R. Matsumoto, M. Yamasaki, M. Otsu, Y. Kawamura, Forgeability and flow stress of Mg-Zn-Y alloys with long period stacking ordered structure at elevated temperatures, Mater. Trans. 50 (2009) 841–846.
[4] M. Yamasaki, T. Anan, S. Yoshimoto, Y. Kawamura, Mechanical properties of warm-extruded Mg–Zn–Gd alloy with coherent 14H long periodic stacking ordered structure precipitate, Scr. Mater. 53 (2005) 799–803.
[5] S. Yoshimoto, M. Yamasaki, Y. Kawamura, Microstructure and mechanical properties of extruded Mg-Zn-Y alloys with 14H long period ordered structure, Mater. Trans. 47 (2006) 959–965.
[6] K. Hagihara, A. Kinoshita, Y. Sugino, M. Yamasaki, Y. Kawamura, H.Y. Yasuda,

Y. Umakoshi, Effect of long-period stacking ordered phase on mechanical properties of Mg97Zn1Y2 extruded alloy, Acta Mater. 58 (2010) 6282–6293.
[7] B. Chen, D. Lin, X. Zeng, C. Lu, Effects of yttrium and zinc addition on the microstructure and mechanical properties of Mg–Y–Zn alloys, J. Mater. Sci. 45 (2010) 2510–2517.
[8] M. Yamasaki, K. Hashimoto, K. Hagihara, Y. Kawamura, Effect of multimodal microstructure evolution on mechanical properties of Mg–Zn–Y extruded alloy, Acta Mater. 59 (2011) 3646–3658.
[9] T. Itoi, T. Inazawa, M. Yamasaki, Y. Kawamura, M. Hirohashi, Microstructure and mechanical properties of Mg–Zn–Y alloy sheet prepared by hot-rolling, Mater. Sci. Eng. A 560 (2013) 216–223.
[10] X.H. Shao, Z.Q. Yang, X.L. Ma, Strengthening and toughening mechanisms in Mg–Zn–Y alloy with a long period stacking ordered structure, Acta Mater. 58 (2010) 4760–4771.
[11] Z.P. Luo, High-resolution electron microscopy on the X-$Mg_{12}ZnY$ phase in a high strength Mg-Zn-Zr-Y magnesium alloy, J. Mater. Sci. Lett. 19 (2000) 813–815.
[12] Y. Chino, M. Mabuchi, S. Hagiwara, H. Iwasaki, A. Yamamoto, H. Tsubakino, Novel equilibrium two phase Mg alloy with the long-period ordered structure, Scr. Mater. 51 (2004) 711–714.
[13] M. Matsuda, S. Ii, Y. Kawamura, Y. Ikuhara, M. Nishida, Variation of long-period stacking order structures in rapidly solidified $Mg_{97}Zn_1Y_2$ alloy, Mater. Sci. Eng. A 393 (2005) 269–274.
[14] T. Itoi, T. Seimiya, Y. Kawamura, M. Hirohashi, Long period stacking structures observed in $Mg_{97}Zn_1Y_2$ alloy, Scr. Mater. 51 (2004) 107–111.
[15] Y.M. Zhu, M. Weyland, A.J. Morton, K. Oh-ishi, K. Hono, J.F. Nie, The building block of long-period structures in Mg–RE–Zn alloys, Scr. Mater. 60 (2009) 980–983.
[16] X. Shao, H. Yang, J.T. De Hosson, X. Ma, Microstructural characterization of long-period stacking ordered phases in $Mg_{97}Zn_1Y_2$ (at%) alloy, Micosc. Microanal. 19 (2013) 1575–1580.
[17] D.H. Ping, K. Hono, Y. Kawamura, A. Inoue, Local chemistry of a nanocrystalline high-strength Mg 97 Y 2 Zn 1 alloy, Philos. Mag. Lett. 82 (2002) 543–551.
[18] E. Abe, Y. Kawamura, K. Hayashi, A. Inoue, Long-period ordered structure in a high-strength nanocrystalline Mg-1 at% Zn-2 at% Y alloy studied by atomic-resolution Z-contrast STEM, Acta Mater. 50 (2002) 3845–3857.
[19] M. Noda, T. Mayama, Y. Kawamura, Evolution of mechanical properties and microstructure in extruded $Mg_{96}Zn_2Y_2$ alloys by annealing, Mater. Trans. 50 (2009) 2526–2531.
[20] M. Yamasaki, K. Hagihara, S.-i. Inoue, J.P. Hadorn, Y. Kawamura, Crystallographic classification of kink bands in an extruded Mg–Zn–Y alloy using intragranular misorientation axis analysis, Acta Mater. 61 (2013) 2065–2076.
[21] D. Egusa, M. Yamasaki, Y. Kawamura, E. Abe, Micro-kinking of the long-period stacking/order(LPSO) phase in a hot-extuded $Mg_{97}Zn_1Y_2$ alloy, Mater. Trans. 54 (2013) 698–702.
[22] K. Hiraga, A. Yasuhara, K. Saito, Dislocations in deformation microstructure of extruded $Mg_{97}Y_2Zn_1$ alloy studied by high-angle annular detector dark-field scanning transmission electron microscopy (HAADF-STEM), Mater. Trans. 53 (2012) 1385–1390.
[23] H. Gao, K.-i. Ikeda, T. Morikawa, K. Higashida, H. Nakashima, Microstructures of long-period stacking ordered phase of Mg–Zn–Y alloy, Mater. Trans. 54 (2013) 632–635.
[24] H. Gao, K.-i. Ikeda, T. Morikawa, K. Higashida, H. Nakashima, Analysis of kink boundaries in deformed synchronized long-period stacking ordered magnesium alloys, Mater. Lett. 146 (2015) 30–33.
[25] X.H. Shao, Z.Z. Peng, Q.Q. Jin, X.L. Ma, Atomic-scale segregations at the deformation-induced symmetrical boundary in an Mg-Zn-Y alloy, Acta Mater. 118 (2016) 177–186.
[26] Y.M. Zhu, A.J. Morton, J.F. Nie, The 18R and 14H long-period stacking ordered structures in Mg–Y–Zn alloys, Acta Mater. 58 (2010) 2936–2947.
[27] S.K. Das, Y.-B. Kang, T. Ha, I.-H. Jung, Thermodynamic modeling and diffusion kinetic experiments of binary Mg–Gd and Mg–Y systems, Acta Mater. 71 (2014) 164–175.
[28] B.Q. Li, M.L. Sui, B. Li, E. Ma, S.X. Mao, Reversible twinning in pure aluminum, Phys. Rev. Lett. 102 (2009) 205504.
[29] J. Geng, M.F. Chisholm, R.K. Mishra, K.S. Kumar, The structure of ⟨c + a⟩ type dislocation loops in magnesium, Philos. Mag. Lett. 94 (2014) 377–386.
[30] Z. Wu, W.A. Curtin, The origins of high hardening and low ductility in magnesium, Nature 526 (2015) 62–67.
[31] M.H. YOO, Slip, twinning, and fracture in hexagonal close-packed metals, Metall. Mater. Trans. A 12A (1981) 409–418.
[32] K. Máthis, K. Nyilas, A. Axt, I. Dragomir-Cernatescu, T. Ungár, P. Lukáč, The evolution of non-basal dislocations as a function of deformation temperature in pure magnesium determined by X-ray diffraction, Acta Mater. 52 (2004) 2889–2894.
[33] X.H. Shao, Z.Q. Yang, X.L. Ma, Interplay between deformation twins and basal stacking faults enriched with Zn/Y in $Mg_{97}Zn_1Y_2$ alloy, Philos. Mag. Lett. 94 (2014) 150–156.
[34] J.-K. Kim, S. Sandlöbes, D. Raabe, On the room temperature deformation mechanisms of a Mg–Y–Zn alloy with long-period-stacking-ordered structures, Acta Mater. 82 (2015) 414–423.
[35] S. Sandlöbes, S. Zaefferer, I. Schestakow, S. Yi, R. Gonzalez-Martinez, On the role of non-basal deformation mechanisms for the ductility of Mg and Mg–Y alloys, Acta Mater. 59 (2011) 429–439.
[36] S. Sandlöbes, M. Friák, S. Zaefferer, A. Dick, S. Yi, D. Letzig, Z. Pei, L.F. Zhu, J. Neugebauer, D. Raabe, The relation between ductility and stacking fault energies in Mg and Mg–Y alloys, Acta Mater. 60 (2012) 3011–3021.
[37] S.R. Agnew, Ö. Duygulu, Plastic anisotropy and the role of non-basal slip in magnesium alloy AZ31B, Int. J. Plast. 21 (2005) 1161–1193.
[38] J.F. Stohr, J.P. Poirier, Etude en microscopie electronique du glissement pyramidal {1122} ⟨1123⟩ dans le magnesium, Philos. Mag. 25 (1972) 1313–1329.
[39] S.R. Agnew, J.A. Horton, M.H. Yoo, Transmission electron microscopy investigation of ⟨c+a⟩ dislocations in Mg and α-solid solution Mg-Li alloys, Metall. Mater. Trans. A 33A (2002) 851–858.
[40] H. Tonda, S. Ando, Effect of temperature and shear direction on yield stress by {11-22} < -1-123 > slip in HCP metals, Metall. Mater. Trans. A 33A (2002) 831–836.
[41] L. Zhou, G. Liu, X.L. Ma, K. Lu, Strain-induced refinement in a steel with spheroidal cementite subjected to surface mechanical attrition treatment, Acta Mater. 56 (2008) 78–87.
[42] X.H. Shao, S.J. Zheng, D. Chen, Q.Q. Jin, Z.Z. Peng, X.L. Ma, Deformation twinning induced decomposition of lamellar LPSO structure and its re-precipitation in an Mg-Zn-Y alloy, Sci. Rep. 6 (2016) 30096. http://dx.doi.org/10.1016/j.actamat.2016.07.054.
[43] A.H. Cottrell, B.A. Bilby, Dislocation theory of yielding and strain ageing of iron, Proc. Phys. Soc. A62 (1949) 49–61.
[44] J.P. Hirth, J. Lothe, Theory of Dislocations, Second ed., Wiley & Sons, New York, 1982.
[45] H. Suzuki, Chemical interaction of solute atoms with dislocations, Sci. Rep. Res. Inst. Tohoku Univ. A4 (1952) 455–463.
[46] W.W. Hu, Z.Q. Yang, H.Q. Ye, Cottrell atmospheres along dislocations in long-period stacking ordered phases in a Mg–Zn–Y alloy, Scr. Mater. 117 (2016) 77–80.
[47] Z. Yang, M.F. Chisholm, G. Duscher, X. Ma, S.J. Pennycook, Direct observation of dislocation dissociation and Suzuki segregation in a Mg–Zn–Y alloy by aberration-corrected scanning transmission electron microscopy, Acta Mater. 61 (2013) 350–359.
[48] Y.M. Zhu, A.J. Morton, M. Weyland, J.F. Nie, Characterization of planar features in Mg–Y–Zn alloys, Acta Mater. 58 (2010) 464–475.
[49] S.K. Das, Y.-M. Kim, T.K. Ha, I.-H. Jung, Investigation of anisotropic diffusion behavior of Zn in hcp Mg and interdiffusion coefficients of intermediate phases in the Mg–Zn system, Calphad 42 (2013) 51–58.
[50] S.K. Das, Y.-B. Kang, T.K. Ha, I.-H. Jung, Thermodynamic modeling and diffusion kinetic experiments of binary Mg–Gd and Mg–Y systems, Acta Mater. 71 (2014) 164–175.
[51] K. Hagihara, Y. Sugino, Y. Fukusumi, Y. Umakoshi, T. Nakano, Plastic deformation behavior of Mg12ZnY LPSO-phase with 14H-typed structure, Mater. Trans. 52 (2011) 1096–1103.
[52] K. Hagihara, T. Okamoto, H. Izuno, M. Yamasaki, M. Matsushita, T. Nakano, Y. Kawamura, Plastic deformation behavior of 10H-type synchronized LPSO phase in a Mg–Zn–Y system, Acta Mater. 109 (2016) 90–102.
[53] J.F. Nie, Y.M. Zhu, J.Z. Liu, X.Y. Fang, Periodic segregation of solute atoms in fully coherent twin boundaries, Science 340 (2013) 957–960.
[54] M. Bugnet, A. Kula, M. Niewczas, G.A. Botton, Segregation and clustering of solutes at grain boundaries in Mg–rare earth solid solutions, Acta Mater. 79 (2014) 66–73.